Hindawi Publishing Corporation
Advances in Condensed Matter Physics
Volume 2014, Article ID 284237, 5 pages
http://dx.doi.org/10.1155/2014/284237

Research Article

Structural and Magnetic Properties of Ni Doped SnO_2

M. Kuppan, S. Kaleemulla, N. Madhusudhana Rao, N. Sai Krishna, M. Rigana Begam, and M. Shobana

Thin Films Laboratory, Materials Physics Division, School of Advanced Sciences, VIT University, Vellore, Tamil Nadu, 632 014, India

Correspondence should be addressed to S. Kaleemulla; skaleemulla@gmail.com

Received 17 May 2013; Accepted 10 December 2013; Published 11 February 2014

Academic Editor: Gary Wysin

Nickel (Ni) doped SnO_2 powder samples were prepared using solid-state reaction with dopant concentrations in the range of 3 at.% to 15 at.%. The influence of Ni doping on structural, optical, and magnetic properties of the powder samples has been investigated. All the Ni doped powder samples exhibited tetragonal structure of SnO_2. A decrease in optical band gap was observed with increase of Ni doping levels. The vibrating sample magnetometer measurements revealed that the Ni doped SnO_2 powder samples were ferromagnetic at room temperature.

1. Introduction

Currently, dilute magnetic semiconductors (DMS) play an important role in spintronic device applications by utilizing both charge and spin degree freedom of the electrons [1]. In DMS, a nonmagnetic semiconductor can be converted into a magnetic semiconductor by introducing a transition metal dopant into a host material. Since the discovery of room temperature ferromagnetism in Mn doped ZnO and GaN by Dietl et al. [2], more attention is being given to DMS to achieve ferromagnetism at room temperature or above room temperature in various oxide semiconductors such as In_2O_3, Cu_2O, TiO_2, and SnO_2. Among these oxide semiconductors, tin oxide (SnO_2) is the most suitable material for many optoelectronic applications. It has a wide band gap (3.5 eV) with high optical transparency in the visible region and high electrical conductivity which are the most essential features for solar cells applications, gas sensors, and liquid crystal displays [3]. A semiconductor that exhibits ferromagnetism along with these properties finds applications in novel magnetic optoelectronic devices. Room temperature ferromagnetism was reported in 3D transition metal doped TiO_2 [4], ZnO [5], Cu_2O [6], and In_2O_3 [7]. Ferromagnetism with a magnetic moment of 0.95 μ_B was reported in Fe doped SnO_2 ceramics by Fitzgerald et al. [8]. But paramagnetic behaviour was reported in the Fe doped SnO_2 by Punnoose et al. [9]. Magnetic properties have been reported in Fe, Mn, and Co doped SnO_2 by many research groups [10–12]. To the best of the authors' knowledge, not much work has been reported on Ni doped SnO_2 semiconductors till date [13]. Hence, an attempt is made here to synthesize Ni doped SnO_2 powders and to study the influence of Ni doping level on structural, optical, and magnetic properties of these powder samples.

2. Materials and Methods

Ni doped SnO_2 powders at 3, 5, 7, 10, and 15 at.% of Ni were prepared by a standard solid-state reaction method. Commercially available SnO_2 and NiO (M/S Sigma-Aldrich, 99.99% pure) were accurately weighed in required proportions using microbalance and were mixed and ground thoroughly using an Agate mortar and pestle to convert to very fine powders. The grinding of the mixture was carried out for 16 h for all the Ni doped SnO_2 powder samples. The ground powder samples were loaded into a small one end closed quartz tube of diameter of 10 mm and length of 10 cm, which was enclosed in a bigger quartz tube of diameter of 2.5 cm and length of 75 cm with provision to allow unwanted vapours to escape from the reaction chamber, and evacuated at 2×10^{-3} mbar using a rotary pump. The complete setup was placed in horizontal tubular

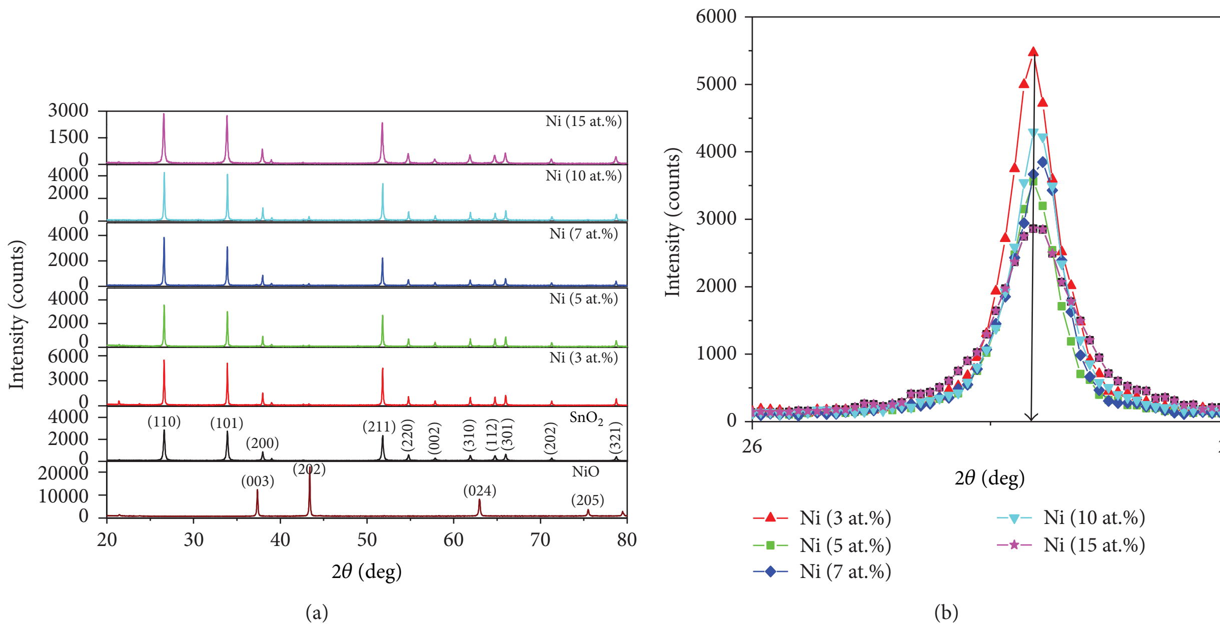

Figure 1: (a) X-ray diffraction patterns of Pure NiO, SnO_2, and Ni doped SnO_2 powder samples at different Ni doping concentrations. (b) XRD patterns of Ni doped SnO_2 powder samples in 2θ range of 26°-27°.

microprocessor controlled furnace and fired for several hours at different temperatures. The firing temperature and firing periods were optimized at 800°C and 10 h through trial- and-error procedures. X-ray diffraction (X-ray diffractometer, D8 Advance, BRUKER) was used to establish structural aspects. The diffused reflectance spectra were recorded using UV-Vis-NIR Spectrophotometer (JASCO V-670). Magnetic measurements were carried out at room temperature using vibrating sample magnetometer (Lake Shore-7404).

3. Results and Discussion

Figure 1(a) shows the X-ray diffraction patterns of undoped and Ni doped SnO_2 powder samples along with X-ray diffraction pattern of pure NiO powder which confirm that the nickel oxide phases were not formed in Ni doped SnO_2 powder samples though the doping level of Ni was increased from 3 at.%. to 15 at.%. All the diffracted peaks of Ni doped SnO_2 powders were indexed based on the unit cell of a tetragonal structure of SnO_2. All the diffracted peaks coincided exactly with tetragonal structure of SnO_2 (JCPDS card number: 411445). As no other peaks related to either nickel or nickel oxides were identified, it could be confirmed that nickel was doped into the host SnO_2 lattice. A high intensity was observed at a Ni doping level of 3 at.%. The intensity of the diffracted peaks and crystallite size showed decrease with increase in Ni doping level. From Figure 1(b), it is clear that the intensity for lower dopant level of 3 at.% is maximum whereas the intensity for the higher dopant level (15 at.%) is minimum, which may be due to impurities that oppose the growth of SnO_2. A decrease in the intensity of the diffracted peaks with the increase of dopant level was also reported in sol-gel synthesized Fe doped SnO_2 [14]. Moreover, no significant shifts in the diffraction angle (2θ) and lattice parameters were observed for the Ni doping levels. It may be due to nearly equal ionic radii of Ni^{+2} ions (0.69 Å) and Sn^{+4} ions (0.71 Å).

Figure 1(b) shows the X-ray diffraction patterns of the Ni doped SnO_2 powder samples in the diffraction angles (2θ) between 26° and 27°. The (1 1 0) orientation for all the Ni doped SnO_2 powder samples was observed between 26.57° and 26.60° of the diffraction angles (2θ). The crystallite size of Ni doped SnO_2 powder samples for all the dopant levels was calculated using Debye-Scherrer formula [15]:

$$L = \frac{k\lambda}{\beta \cos\theta}, \quad (1)$$

where k is a constant, λ is the diffraction wavelength of CuK_α ($\lambda = 1.5406$ Å), β is the full width at half maximum (FWHM), and θ is the diffracted angle, respectively. The crystallite size, lattice parameter, and unit cell volume showed decrease from 81 nm to 67 nm, 4.740 Å to 4.736 Å, and 71.592 Å^3 to 71.438 Å^3, respectively, with the increase of Ni doping level from 3 at.% to 10 at.%. The FWHM of the Ni doped SnO_2 powders showed increase from 0.105 to 0.126 with the increase of Ni doping level from 3 at.% to 10 at.%. The tetragonal distortion (c/a) increased from 0.672 to 0.673 with the increase of Ni doping level from 3 at.% to 15 at.%. The crystallite size, lattice parameter, and unit cell volume exhibited increase again when the Ni doping level has increased to 15 at.%. It suggests that Ni at 10 at.% is the doping limit in SnO_2 lattice. All these changes indicate that the doping of Ni took place in SnO_2 lattice. A summary of Ni doping levels (at.%), full width at half maximum (FWHM), 2θ (1 1 0) from XRD, grain size (L), lattice parameters, tetragonal distortion (c/a), and unit cell volume (V) is given in Table 1.

Table 1: Summary of doping concentrations (at.%), FWHM, 2θ (1 1 0) from XRD, grain size (L), lattice parameters, tetragonal distortion (c/a), and unit cell volume (V) of Ni doped SnO_2 powder samples.

Ni (at.%)	FWHM	2θ	L (nm)	a (Å)	c (Å)	c/a	V (Å^3)
3	0.105	26.57	81	4.740	3.185	0.672	71.592
5	0.112	26.59	76	4.737	3.184	0.672	71.460
7	0.118	26.57	72	4.739	3.185	0.672	71.548
10	0.126	26.59	67	4.736	3.185	0.672	71.438
15	0.115	26.60	74	4.734	3.186	0.673	71.442

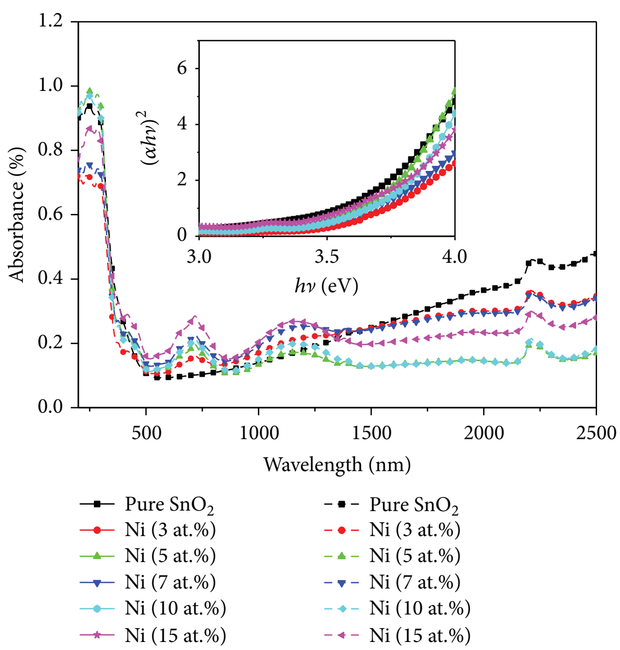

Figure 2: Optical absorbance spectra of Ni doped SnO_2 powder samples. Inset figure shows the optical band gaps of the Ni doped SnO_2 powder samples.

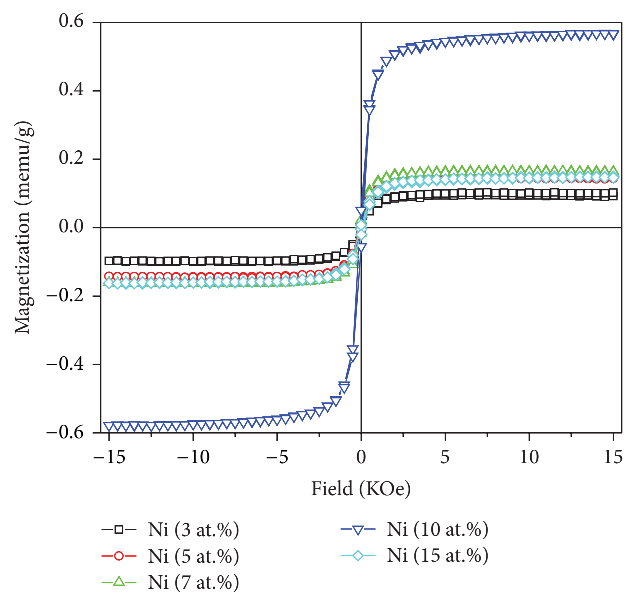

Figure 3: *M-H* plots of Ni doped SnO_2 powder samples at different Ni dopant concentrations.

In order to study the influence of Ni doping levels on the optical band gap, absorbance spectra were recorded for all Ni doped SnO_2 powder samples. Figure 2 shows the optical absorbance spectra of pure SnO_2 and Ni doped SnO_2 powder samples at different Ni doping levels. The undoped SnO_2 powder exhibited a minimum absorbance at a wavelength of 500 nm. When Ni doping level has increased the absorbance of the samples showed an increase and touched a maximum value at Ni doping level of 15 at.%. It may be due to the dopant impurities which could increase absorbance. Additional bands have been observed at wavelength of 721 nm for all Ni doping concentrations. It may be due to the substitution of Ni in SnO_2 lattice. The absorption coefficient (α) of the powder samples was calculated using the following relation:

$$\alpha = 2.303\frac{a}{t}, \tag{2}$$

where "a" is the absorbance and "t" is the path length. The optical band gap (E_g) for a highly degenerate semiconducting oxide can be determined from the absorption coefficient (α) and photon energy (hv) using the following relation [16]:

$$\alpha hv = A\left(E_g - hv\right)^{1/2}. \tag{3}$$

The optical bang gap (E_g) was calculated by plotting $(\alpha hv)^2$ versus the photon energy (hv) and by extrapolating the linear region of the plots to zero absorption ($\alpha = 0$). The optical band gap of the powder samples decreased from 3.76 eV to 3.70 eV when the Ni dopant level was increased from 3 at.% to 15 at.%. The optical band gap energy shows a narrowing effect with increase in Ni dopant level. Similar results were reported in Ni doped SnO_2 nanoparticles by Ahmed et al. [17]. A decrease in optical band gap with doping level has been explained by many groups who suggested the alloying effect in the host compound with some impurity phases [18].

Figure 3 shows the magnetization versus magnetic field curves of the Ni doped SnO_2 powder samples at different dopant levels. The pure SnO_2 powder exhibited diamagnetic behavior at room temperature. When Ni was doped into SnO_2 lattice, a change in magnetization was observed. The substitution of Ni ion with SnO_2 matrix transformed it from its diamagnetic state to ferromagnetic state.

Table 2: Summary of doping concentrations (at.%), saturation magnetization (M_s), coercivity (H_{ci}), retentivity (M_r), magnetic susceptibility (χ), and magnetic moment per Ni atom (μ_B/Ni) of the Ni doped SnO_2 powder samples.

Ni (at.%)	M_s (memu/g)	H_{ci} (Oe)	M_r (memu/g)	χ ($\times 10^{-6}$)	μ_B/Ni
3	0.101	68.68	0.007	6.7	3.02×10^{-3}
5	0.148	79.75	0.014	9.9	2.66×10^{-3}
7	0.164	82.49	0.019	10.9	2.10×10^{-3}
10	0.573	65.75	0.052	38.2	5.15×10^{-3}
15	0.156	78.32	0.013	10.4	9.35×10^{-4}

The saturation magnetization (M_s), retentivity, and coercivity were also found to be increased with increase in dopant levels. The ferromagnetic signal is progressively enhanced up to 10 at.% of dopant. A magnetic moment of 0.101 memu/g and coercivity of 65.8 Oe were observed in Ni doped SnO_2 powder at a 3 at.% of dopant level. The highest saturation magnetic moment of 0.573 memu/g and coercive field of 65.75 Oe were observed for the powder sample 10 at.% dopant level. It may be due to substitution of Ni^{2+} with Sn^{4+} which favours an increase of oxygen vacancies available for electron trapping and hence increase in saturation magnetic moment at 10 at.% of Ni doped SnO_2 powders. The observed saturation magnetic moments are lower when compared with saturation magnetic moments of Co and Fe doped SnO_2 by Kaur et al. [19] and single crystal Co doped SnO_2 nanocrystals by Xu et al. [20]. A ferromagnetic behavior at lower concentrations and paramagnetic behavior at higher doping concentration were reported in Ni doped SnO_2 nanocrystals by Aragón et al. [21]. But in the present system, ferromagnetism has been observed even at higher Ni doping levels but the saturation magnetic moment decreased at higher dopant levels (15 at.%). A summary of crystallite size, saturation magnetization (M_s), coercivity (H_{ci}), retentivity (M_r), magnetic susceptibility (χ), and magnetic moment per Ni ion (μ_B/Ni) of the Ni doped SnO_2 powder samples is given in Table 2.

4. Summary and Conclusions

Ni doped SnO_2 powder samples were synthesized using solid-state reaction method. The dopant levels were varied from 3 at.% to 15 at.%. All the Ni doped SnO_2 powder samples showed tetragonal structure. No new phases of either NiO or SnO were found even at higher dopant levels (15 at.%). The optical band gap decreased from 3.76 eV to 3.70 eV with the increase of Ni from 3 at.% to 15 at.%. The room temperature ferromagnetism was found in all Ni doped SnO_2 powder samples. The Ni doped SnO_2 powder samples exhibited the highest saturation magnetic moment of 0.573 memu/g at a Ni doping level of 10 at.%.

Conflict of Interests

The authors declare that there is no conflict of interests regarding the publication of this paper.

Acknowledgments

Authors are highly thankful to VIT-SIF for providing XRD and DRS facilities to carry out the present work. Authors also thank Sophisticated Advanced Instruments Facility (SAIF), IIT Madras, Tamil Nadu, India, for providing vibrating sample magnetometer facility.

References

[1] H. Ohno, "Making nonmagnetic semiconductors ferromagnetic," *Science*, vol. 281, no. 5379, pp. 951–956, 1998.

[2] T. Dietl, H. Ohno, F. Matsukura, J. Cibert, and D. Ferrand, "Zener model description of ferromagnetism in zinc-blende magnetic semiconductors," *Science*, vol. 287, no. 5455, pp. 1019–1022, 2000.

[3] S. H. Mohamed, "SnO_2 dendrites-nanowires for optoelectronic and gas sensing applications," *Journal of Alloys and Compounds*, vol. 510, no. 1, pp. 119–124, 2011.

[4] A. Kaushik, B. Dalela, S. Kumar, P. A. Alvi, and S. Dalela, "Role of Co doping on structural, optical and magnetic properties of TiO_2," *Journal of Alloys and Compounds*, vol. 552, pp. 274–278, 2013.

[5] R. Saleh, N. F. Djaja, and S. P. Prakoso, "The correlation between magnetic and structural properties of nanocrystalline transition metal-doped ZnO particles prepared by co-precipitation method," *Journal of Alloys and Compounds*, vol. 546, pp. 48–56, 2013.

[6] F. Jlaiel, M. Amami, N. Boudjada, P. Strobel, and A. Ben Salah, "Metal transition doping effect on the structural and physical properties of delafossite-type oxide $CuCrO_2$," *Journal of Alloys and Compounds*, vol. 509, no. 29, pp. 7784–7788, 2011.

[7] S. Khatoon, K. Coolahan, S. E. Lofland, and T. Ahmad, "Optical and magnetic properties of solid solution of $In_{2-x}Mn_xO_3$ (0.05, 0.10 and 0.15) nanoparticles," *Journal of Alloys and Compounds*, vol. 545, pp. 162–167, 2012.

[8] C. B. Fitzgerald, M. Venkatesan, A. P. Douvalis, S. Huber, J. M. D. Coey, and T. Bakas, "SnO_2 doped with Mn, Fe or Co: room temperature dilute magnetic semiconductors," *Journal of Applied Physics*, vol. 95, no. 11, pp. 7390–7392, 2004.

[9] A. Punnoose, J. Hays, A. Thurber, M. H. Engelhard, R. K. Kukkadapu, and C. Wang, "Development of high temperature ferromagnetism in SnO_2 and paramagnetism in SnO by Fe doping," *Physical Review B*, vol. 72, no. 5, Article ID 054402, 14 pages, 2005.

[10] L. M. Fang, X. T. Zu, Z. J. Li et al., "Synthesis and characteristics of Fe^{3+}-doped SnO_2 nanoparticles via sol-gel-calcination or sol-gel-hydrothermal route," *Journal of Alloys and Compounds*, vol. 454, no. 1-2, pp. 261–267, 2008.

[11] Z. M. Tian, S. L. Yuan, J. H. He et al., "Structure and magnetic properties in Mn doped SnO_2 nanoparticles synthesized by chemical co-precipitation method," *Journal of Alloys and Compounds*, vol. 466, no. 1-2, pp. 26–30, 2008.

[12] H. Wang, Y. Yan, Y. S. Mohammed, X. Du, K. Li, and H. Jin, "The role of Co impurities and oxygen vacancies in the ferromagnetism of Co-doped SnO_2: GGA and GGA+U studies," *Journal of Magnetism and Magnetic Materials*, vol. 321, no. 19, pp. 3114–3119, 2009.

[13] J. Zhang, Q. Yun, and Q. Wang, "Room temperature ferromagnetism of Ni-doped SnO_2 system," *Modern Applied Science*, vol. 4, no. 11, pp. 124–130, 2010.

[14] K. Nomura, C. A. Barrero, J. Sakuma, and M. Takeda, "Room temperature ferromagnetism of sol-gel synthesized $Sn_{1-x}57Fe_xO_{2-\delta}$ powders," *Phys. Review B*, vol. 75, no. 18, Article ID 184411, 13 pages, 2007.

[15] B. D. Cullity, *Elements of X-Ray Diffraction*, Addison-Wesley, Reading, Mass, USA, 1972.

[16] J. Tauc, *Amorphous and Liquid Semiconductors*, Plenum Press, New York, NY, USA, 1974.

[17] A. S. Ahmed, M. M. Shafeeq, M. L. Singla, S. Tabassum, A. H. Naqvi, and A. Azam, "Band gap narrowing and fluorescence properties of nickel doped SnO_2 nanoparticles," *Journal of Luminescence*, vol. 131, no. 1, pp. 1–6, 2011.

[18] N. Barreau, J. C. Bernède, S. Marsillac, and A. Mokrani, "Study of low temperature elaborated tailored optical band gap β-$In_2S_{3-3x}O_{3x}$ thin films," *Journal of Crystal Growth*, vol. 235, no. 1–4, pp. 439–449, 2002.

[19] J. Kaur, J. Shah, R. K. Kotnala, and K. C. Verma, "Raman spectra, photoluminescence and ferromagnetism of pure, Co and Fe doped SnO_2 nanoparticles," *Ceramics International*, vol. 38, no. 7, pp. 5563–5570, 2012.

[20] Y. Xu, Y. Tang, C. Li et al., "Synthesis and room-temperature ferromagnetic properties of single-crystalline Co-doped SnO_2 nanocrystals via a high magnetic field," *Journal of Alloys and Compounds*, vol. 481, no. 1-2, pp. 837–840, 2009.

[21] F. H. Aragón, J. A. H. Coaquira, P. Hidalgo, S. L. M. Brito, D. Gouvêa, and R. H. R. Castro, "Experimental study of the structural, microscopy and magnetic properties of Ni-doped SnO_2 nanoparticles," *Journal of Non-Crystalline Solids*, vol. 356, no. 52–54, pp. 2960–2964, 2010.